PCCP

RSC Publishing

PAPER

View Article Online
View Journal | View Issue

Cite this: *Phys. Chem. Chem. Phys.*, 2013, **15**, 17636

Production of gas phase NO_2 and halogens from the photolysis of thin water films containing nitrate, chloride and bromide ions at room temperature†

Nicole K. Richards-Henderson,[a] Karen M. Callahan,[a] Paul Nissenson,[b] Noriko Nishino,[a] Douglas J. Tobias*[a] and Barbara J. Finlayson-Pitts*[a]

Received 15th July 2013,
Accepted 4th September 2013

DOI: 10.1039/c3cp52956h

www.rsc.org/pccp

Nitrate and halide ions coexist in particles generated in marine regions, around alkaline dry lakes, and in the Arctic snowpack. Although the photochemistry of nitrate ions in bulk aqueous solution is well known, there is recent evidence that it may be more efficient at liquid–gas interfaces, and that the presence of other ions in solution may enhance interfacial reactivity. This study examines the 311 nm photolysis of thin aqueous films of ternary halide–nitrate salt mixtures (NaCl–NaBr–$NaNO_3$) deposited on the walls of a Teflon chamber at 298 K. The films were generated by nebulizing aqueous 0.25 M $NaNO_3$ solutions which had NaCl and NaBr added to vary the mole fraction of halide ions. Molar ratios of chloride to bromide ions were chosen to be 0.25, 1.0, or 4.0. The subsequent generation of gas phase NO_2 and reactive halogen gases (Br_2, BrCl and Cl_2) were monitored with time. The rate of gas phase NO_2 formation was shown to be enhanced by the addition of the halide ions to thin films containing only aqueous $NaNO_3$. At $[Cl^-]/[Br^-] \leq 1.0$, the NO_2 enhancement was similar to that observed for binary NaBr–$NaNO_3$ mixtures, while with excess chloride NO_2 enhancement was similar to that observed for binary NaCl–$NaNO_3$ mixtures. Molecular dynamics simulations predict that the halide ions draw nitrate ions closer to the interface where a less complete solvent shell allows more efficient escape of NO_2 to the gas phase, and that bromide ions are more effective in bringing nitrate ions closer to the surface. The combination of theory and experiments suggests that under atmospheric conditions where nitrate ion photochemistry plays a role, the impact of other species such as halide ions should be taken into account in predicting the impacts of nitrate ion photochemistry.

1. Introduction

The loss of nitrogen species to sea salt aerosols through heterogeneous reactions is an important removal pathway for NO_y (N_2O_5, NO_2, HNO_3 and $ClONO_2$) in the marine troposphere.[1–29] Nitrate formed from these reactions is a common constituent of sea salt aerosols (100–400 mM)[30] and is one of the most abundant soluble anions in high-latitude snow and ice.[31,32]

Nitrate photolyzes in the actinic region above 290 nm[33–37] and is known to be a major source of NO_x as well as OH and $O(^3P)$ in the condensed phase[30,38–49] including on polar snowpacks and in laboratory studies of frozen nitrate solutions:[50–57]

$$NO_3^- + h\nu \rightarrow NO_2 + O^- \quad (1a)$$

$$NO_3^- + h\nu \rightarrow NO_2^- + O(^3P) \quad (1b)$$

$$O^- + H_2O \rightarrow OH + OH^- \quad (k_2 = 9.3 \times 10^7\ M^{-1}\ s^{-1})^{58} \quad (2)$$

In bulk solutions at room temperature, the quantum yield at 305 nm is $\phi \sim 0.01$ for OH production *via* reactions (1a) and (2) and an order of magnitude lower ($\phi \sim 0.001$) for $O(^3P)$ formation in (1b).[33–37] The OH radical formed from the O^- reaction[58] with H_2O oxidizes Br^- and Cl^- to form Br_2, Cl_2 and BrCl.[30,59–71] These reactive halogen gases play a significant role in the chemistry and composition of the marine boundary layer (MBL).[45,72–81] In the coastal MBL, the photochemical cycling of chlorine enhances tropospheric ozone, whereas gaseous bromine species cause ozone destruction during polar sunrise in polar regions[75,76,82–85] as well as in mid-latitudes.[78–81,86,87] However, despite laboratory and field measurements of halogen gases, the mechanisms responsible for halogen release, including those associated with reactive intermediates from nitrate ion photochemistry, are not well understood.[74,88–98]

[a] *Department of Chemistry, University of California, Irvine, CA 92697-2025, USA. E-mail: bjfinlay@uci.edu, dtobias@uci.edu; Fax: +1-949-824-2420; Tel: +1-949-824-7670, +1-949-824-4295*

[b] *Department of Mechanical Engineering, California State Polytechnic University, Pomona, CA 91768-4062, USA*

† Electronic supplementary information (ESI) available. See DOI: 10.1039/c3cp52956h

Previous studies in this laboratory established that the photolysis of deliquesced aerosols of $NaNO_3$ deposited on a Teflon substrate, with either added chloride[99] or bromide ions,[100] showed an enhancement in NO_2 production in the presence of halide ions. The enhancement upon addition of synthetic sea salt was also shown to be similar to that for NaCl–$NaNO_3$ mixtures.[101] When bromide ions were present, gas phase Br_2 was generated. The increase in NO_2 production was attributed to the presence of halide ions at the solution–air interface which draw sodium ions toward the surface in a double-layer effect, which in turn attracts nitrate ions. Because of their proximity to the interface, these nitrate ions have a less complete solvent cage than in the bulk phase. The recombination of the reactive fragments initially generated is less efficient, resulting in greater escape of NO_2 to the gas phase. Consistent with the bromide ion effect, Donaldson and coworkers[102] have recently used glancing-angle Raman spectroscopy to detect an enhancement in nitrate ions at the surface of aqueous mixtures of $NaNO_3$ with NaBr. Interestingly, and inconsistent with the photochemistry experiments and molecular dynamics (MD) simulations, no enhancement was observed with chloride ions.

The goal of the present work is to analyze the impact of chloride and bromide ions on the production of gas phase NO_2 and halogens when these anions are simultaneously present. Elucidating the chemistry and photochemistry of such mixtures is critical for interpreting and modeling the chemistry of sea salt aerosols in air or deposited on the snowpack or other surfaces. The competition between chloride and bromide ions for the reactive intermediates generated in the nitrate ion photolysis, Cl^-–Br^- interhalogen chemistry, and the ability of the competing co-anions to draw nitrate towards the interface *via* the double-layer effect can greatly complicate the understanding of NO_2 formation in NaCl–NaBr–$NaNO_3$ systems compared to systems with only single halides. In the present study, a combination of experimental and theoretical approaches are used to examine the impact of these processes on NO_2 formation.

2. Materials and methods

Photolysis experiments

Photolysis experiments were carried out using 230 L Teflon (51 μm FEP) reaction chambers. The procedure for coating the reaction chambers with salt solutions by a nebulizer is described in detail elsewhere.[100] After being coated with salt, the chambers were filled with synthetic air (Scott-Marrin, Riverside, CA; $NO_x < 0.001$ ppm, $SO_2 < 0.001$ ppm) that had flowed through a water bubbler to obtain a final relative humidity of 75–78% measured using a relative humidity-temperature probe (Vaisala, HMP 338). The chambers were irradiated with 14 externally mounted narrowband UVB lamps ($\lambda \sim 311$ nm, Phillips TL 20 W/01 RS), whose output overlaps with the n → π* absorption band of nitrate (for lamp spectra see ref. 100). Experiments were conducted at 298 ± 2 K.

Gas phase NO_2 and NO were monitored as a function of time by periodically sampling from the Teflon chamber into a nitrogen oxides analyzer with chemiluminescence detection (ThermoElectron Corp., Model 42C) and into a 28 m multiple reflection White cell optical system[103] interfaced to a Fourier transform infrared absorption spectrometer (Mattson, Infinity 60AR). Infrared spectra were recorded at a resolution of 0.5 cm^{-1} with 1024 co-added scans. Both the nitrogen oxides analyzer and FTIR were calibrated in the range of NO_2 levels detected in the experiments using known mixtures of NO_2 prepared by further diluting an initial mixture of 4.57 NO_2 ppmv (Scott-Marrin Inc.) in oxygen-free N_2 with N_2 (Oxygen Service Co., UHP, 99.999%).

An atmospheric pressure chemical ionization triple quadrupole mass spectrometer (API-MS) (Perkin-Elmer Sciex, API-300) was used to quantify Br_2, BrCl, and Cl_2 production. Two mass spectrometry scan modes were utilized in this study, single quadrupole (Q1) and multiple reactions monitoring (MRM), both in the negative ionization mode. Q1 scans monitored ions in a selected range of mass to charge ratios (m/z 30–500 amu) using a single quadrupole. Confirmation of the products was achieved using the MRM technique in which an ion selected using the first quadrupole was collisionally dissociated and the fragments separated and identified using the second quadrupole. Parent–daughter ion pairs that were monitored during photolysis experiments were 158/79 and 160/81 for Br_2, 70/35 and 72/35 for Cl_2, and 114/79 and 114/35 for BrCl. Calibrations were carried out using known concentrations of gaseous Br_2 or Cl_2 obtained by flowing measured volumes of Br_2 (Acros, 99.8%) or Cl_2 (Matheson Tri Gas, Inc.) into a Teflon chamber with a known volume of air. The calibration for BrCl was assumed to be the same as for Cl_2 based on previous laboratory studies in which sensitivities were within 15%.[82]

The salts $NaNO_3$ (Fisher, Certified ACS, >99.0%), NaCl (Fluka, >99.5%), and NaBr (Fluka, >99.5%) were used as received from the manufacturers and solutions were made using Milli-Q water (Millipore, 18.2 MΩ cm, pH 5.5). Experiments on mixtures of NaCl–NaBr–$NaNO_3$ were carried out by varying the total halide content ($Cl^- + Br^-$) from 0.083 M to 2 M. The total concentration of chloride plus bromide ions relative to nitrate ions is expressed throughout the paper using the halide mole fraction, χ_{halide}, defined as:

$$\chi_{halide} = \frac{[Cl^-] + [Br^-]}{[Cl^-] + [Br^-] + [NO_3^-]}$$

The ratio of chloride to bromide ions was varied, with $[Cl^-]/[Br^-]$ = 0.25, 1.0, and 4.0, respectively. The nitrate concentration in the nebulizer was held constant for all experiments at 0.25 M. Irradiation experiments were also conducted for thin films of 4 M NaCl, 4 M NaBr, and mixtures of NaBr and NaCl (2 M each) as well as for Teflon reaction chambers with no salt added. In all of these experiments neither NO_x or halogen gas was detected.

Errors in concentrations are reported as 2s, where s is the sample standard deviation defined as

$$s = \sqrt{\frac{\left(\sum_{i=1}^{N} (x_i - \bar{x})^2\right)}{N-1}}$$

where N is the number of samples and was 3–5 depending on the measurement.[104]

Scanning electron microscopy (SEM)

A scanning electron microscope (Zeiss Evo LS 15) equipped with a Thermo Electron Corporation Ultra Dry Silicon Drift energy dispersive X-ray spectroscopy (EDS) detector was used to investigate the morphology and elemental composition of thin films of NaCl–NaBr–$NaNO_3$. An accelerating electron beam voltage of 8 keV was used. The thin films were prepared on copper stubs (Ted Pella Inc.) which were placed inside a Teflon reaction chamber and subjected to preparation as described previously.[100] SEM images were taken after the last evacuation but before the rehumidification step.

MD simulations

Liquid–vapor interfaces containing mixtures of NaCl–NaBr–$NaNO_3$, and aqueous $NaNO_3$ were simulated using slab geometry[105,106] in which unit cells of 30 Å × 30 Å × 100 Å were replicated using three-dimensional periodic boundary conditions.[107] All slab simulations contained 864 water molecules and the sum of 72 cation–anion pairs: NaCl, NaBr, and $NaNO_3$. All simulations were run in the NVT (constant moles, volume, and temperature) ensemble using a temperature of 300 K after equilibration using the Berendsen thermostat.[108] All simulations incorporated the polarizable POL3 water model.[109,110] Water bond lengths and angles were constrained using the SHAKE algorithm.[110] The sodium, bromide, and chloride parameters were adapted from the work of Berkowitz and coworkers.[111,112] The nitrate force field was modeled using parameters by Thomas *et al.*,[113] which combines Lennard-Jones parameters from Minofar *et al.*[114] and polarizability parameters by Salvador *et al.*[115] The ion and water force field parameters are provided in Table S1 (ESI†). The MD program employed was Sander in the AMBER 8 suite[116] of programs, using a version that has a modified calculation of the induced dipoles which was introduced to avoid ''polarization catastrophe'' in solutions with nitrate.[117] Particle-mesh Ewald summation was used to treat the long-range electrostatic interactions.[118,119] The real-space part of the Ewald sum and the Lennard Jones interactions were cut off at 12 Å. The time-step was 1 fs and trajectory data were recorded every picosecond. Each simulation was equilibrated for 2 ns and an additional 10 ns were used for analysis. Table 1 summarizes the numbers of each anion used along with 72 Na^+ and 864 water molecules in the simulations of the various mixtures. The solvation environment around nitrate ions was investigated for the mixtures of NaCl–NaBr–$NaNO_3$ by calculating the number of water molecules within 5.5 Å of the nitrogen of NO_3^- as a function of depth into the slab.

Table 1 Numbers of anions used for MD simulations in mixtures with 864 water molecules and 72 Na^+ to represent solutions used in the experiments

$\chi_{NaCl+NaBr}$	Number of Cl^- and Br^-	Number of NO_3^-
0[a]	0	72
0.5[b]	36	36
0.75[b]	54	18
0.9[b]	65	7

[a] Corresponds to 4 M $NaNO_3$. [b] For each condition, molar ratios corresponding to $[Cl^-]/[Br^-]$ = 0.25, 1.0, and 4.0 were simulated to match the experimental conditions.

Chemical kinetics model

A computational chemical kinetics box model was used to explore the mechanisms of Br_2 and NO_2 production in these systems. The model was created using the FACSIMILE integrator (MCPA software) and includes 128 gas-phase reaction rate constants (Table S2, ESI†), 182 aqueous-phase reaction rate constants (Table S3, ESI†), 25 Henry's law constants (Table S4, ESI†) and 20 photolysis rate constants (Table S5, ESI†). Transport between the gas and aqueous phase was governed by instantaneous Henry's law equilibrium. The model was parameterized by adjusting the rate constant of the two nitrate photolysis channels ((1a) and (1b)) in order to change the quantum yield of nitrate photolysis products. The rate of the two nitrate photolysis channels was adjusted until simulated NO_2 concentrations matched experimental observations.

3. Results and discussion

Photolysis experiments on thin films of NaCl–NaBr–$NaNO_3$ were carried out with constant initial nitrate concentrations, while the ratios of chloride and bromide ions were varied so that $[Cl^-]/[Br^-]$ = 0.25, 1.0, and 4.0. Fig. 1 shows gas phase NO_2 concentrations increased as a function of photolysis time and as the mole fraction of added halide ions, χ_{halide}, increased. Clearly, the addition of the halide ions substantially increases NO_2 production. While the rates of NO_2 generation are similar to each other for $[Cl^-]/[Br^-]$ = 0.25 and 1.0, they are lower for a ratio of 4.0. The rates of NO_2 generation are summarized and compared in Table 2 to those from binary mixtures of NaCl–$NaNO_3$ and NaBr–$NaNO_3$ reported earlier.[99,100]

Fig. 2a compares the rates of NO_2 production as a function of χ_{halide} for photolysis of thin films containing $[Cl^-]/[Br^-]$ = 4.0 (red squares) and previously reported NaCl–$NaNO_3$ (blue triangles) experiments.[99] The magnitudes of the rates of NO_2 production for the ternary NaCl–NaBr–$NaNO_3$ mixture and the trends with χ_{halide} are very similar to those previously measured for binary NaCl–$NaNO_3$ mixtures (blue triangles). Thus, the addition of small amounts of bromide ions to NaCl–$NaNO_3$ solutions has minimal impact on the rate of release of NO_2. This is consistent with studies on the photolysis of mixtures of synthetic sea salt ($[Cl^-]/[Br^-]$ = 660) and $NaNO_3$ which were within experimental error of NaCl–$NaNO_3$.[101]

Fig. 2b compares the rates of NO_2 production from the ternary mixtures with higher relative bromide concentrations, *e.g.*, $[Cl^-]/[Br^-]$ = 1.0 (green squares) and 0.25 (orange triangles), to those from NaBr–$NaNO_3$ (pink circles). The NO_2 production rate from the ternary mixture is similar to that for NaBr–$NaNO_3$ except for χ_{halide} = 0.25–0.5. As discussed elsewhere,[100] some segregation of halide and nitrate was thought to occur in the binary NaBr–$NaNO_3$ mixtures over the

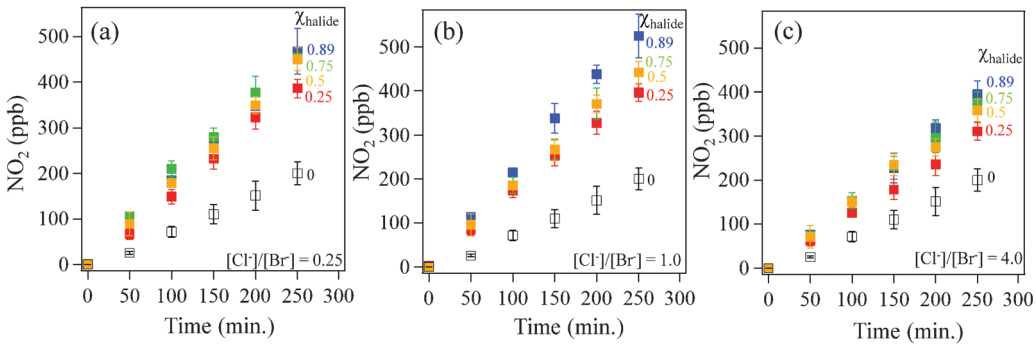

Fig. 1 NO_2 production during photolysis experiments of pure $NaNO_3$ (open black squares) and mixtures of NaCl–NaBr–$NaNO_3$ for (a) $[Cl^-]/[Br^-]$ = 0.25, (b) $[Cl^-]/[Br^-]$ = 1.0 and (c) $[Cl^-]/[Br^-]$ = 4.0 at 75–78% RH and 298 K in air, where χ_{halide} is the mole fraction of NaCl + NaBr.

Table 2 Rates of NO_2 production[a] from photolysis of NaCl–NaBr–$NaNO_3$ mixtures as function of χ_{halide} for $[Cl^-]/[Br^-]$ = 0.25, 1.0, and 4.0

Halide mole fraction	$[Cl^-]/[Br^-]$ ratio in NaCl–NaBr–$NaNO_3$ mixtures				
χ_{halide}	0.25	1	4	NaCl–$NaNO_3$[b]	NaBr–$NaNO_3$[b]
0	0.81 ± 0.05	0.81 ± 0.05	0.81 ± 0.05	0.75 ± 0.05	0.81 ± 0.05
0.1	nd[c]	nd	nd	1.20 ± 0.05	nd
0.25	1.61 ± 0.11	1.71 ± 0.10	1.21 ± 0.08	nd	1.02 ± 0.1
0.5	1.79 ± 0.08	1.80 ± 0.11	1.39 ± 0.08	1.33 ± 0.05	1.11 ± 0.1
0.75	1.81 ± 0.08	1.88 ± 0.05	1.51 ± 0.08	1.45 ± 0.05	1.62 ± 0.1
0.9	1.83 ± 0.12	2.2 ± 0.10	1.62 ± 0.08	1.9 ± 0.02	1.92 ± 0.1

[a] Rates are in units of ppb min^{-1}. [b] Rates from binary NaCl–$NaNO_3$ and NaBr–$NaNO_3$ mixtures measured previously[99,100] were normalized to correspond to the present experiments. [c] nd = not determined.

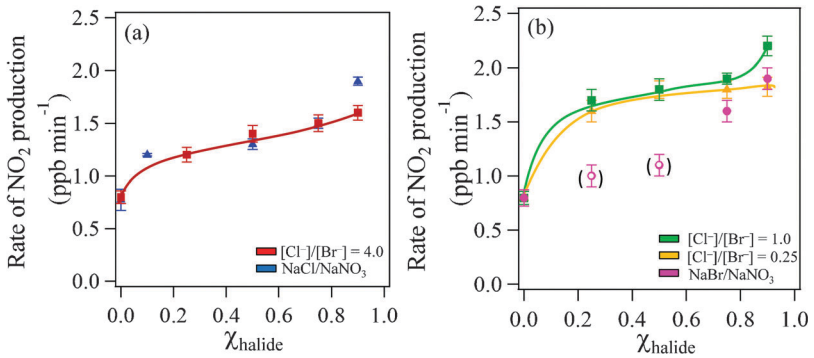

Fig. 2 Rates of production of NO_2 from mixtures of NaCl–NaBr–$NaNO_3$ as a function of χ_{halide} for (a) $[Cl^-]/[Br^-]$ = 4.0 (red) and NaCl–$NaNO_3$ (blue) and (b) $[Cl^-]/[Br^-]$ = 0.25 (orange) and 1.0 (green) and NaBr–$NaNO_3$ (pink). The NaCl–$NaNO_3$ and NaBr–$NaNO_3$ experiments have been normalized to the same initial nitrate ion concentrations as used in the present experiments. Error bars represent 2*s* of replicate experiments.

range χ_{NaBr} = 0.25–0.5, resulting in artificially low rates of NO_2 production. In the present studies, scanning electron microscopy images (Fig. 3 and Fig. S1 in ESI†) of thin films of the salts on copper stubs show that the halide and nitrate ions are generally co-located for the ternary mixtures, indicating that segregation is not as severe as in the binary mixtures. (It is assumed that SEM images of thin films of salt collected on the copper stubs are representative of the same films collected on the Teflon substrate). Thus the presence of chloride ions appears to minimize segregation of the anions and the resulting rates of NO_2 production reflect those from well-mixed salts. The similarity of the rate of production of NO_2 between the ternary mixture and NaBr–$NaNO_3$ at high halide mole fractions suggests that the data for χ_{halide} = 0.25–0.5 are what would have been observed for the binary NaBr–$NaNO_3$ mixtures had segregation of the salts not occurred.

The increased rates of NO_2 production in the $[Cl^-]/[Br^-]$ = 0.25 and 1.0 systems (Fig. 2b) relative to $[Cl^-]/[Br^-]$ = 4.0 (Fig. 2a) may be due to higher interfacial concentrations of nitrate due to larger Br^- concentrations at the solution interface compared to chloride. To assess this possibility, MD simulations were conducted on ternary mixtures of NaCl–NaBr–$NaNO_3$ with molar ratios corresponding to $[Cl^-]/[Br^-]$ = 0.25, 1.0, and 4.0, as in the experiments. The density profiles were normalized so the area under each curve was 0.5, and then shifted along the *z*-axis until the Gibbs dividing surface (GDS)

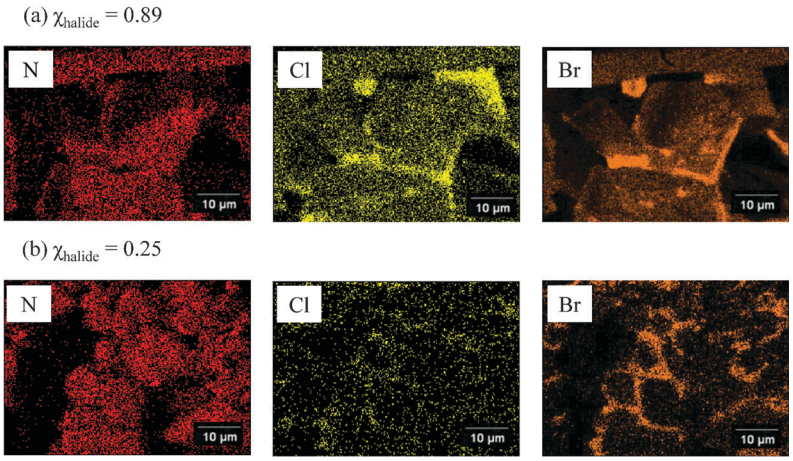

Fig. 3 Element maps for NaCl–NaBr–$NaNO_3$ mixtures with (a) χ_{halide} = 0.89 and (b) χ_{halide} = 0.25. In all cases, $[Cl^-]/[Br^-]$ = 1.0.

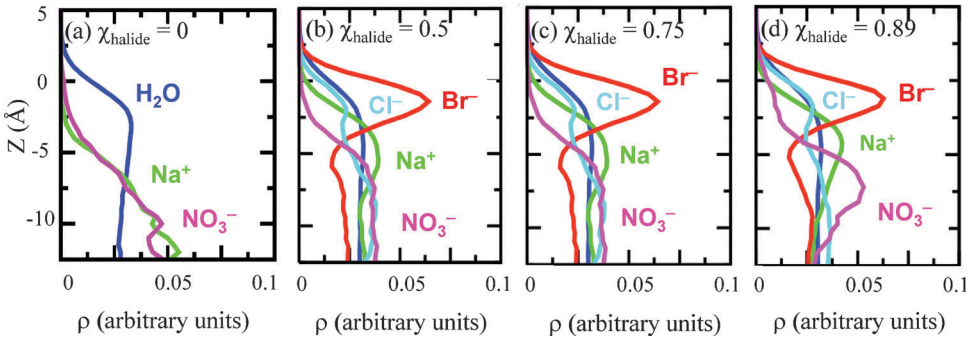

Fig. 4 Density profiles from the MD simulations of NaCl–NaBr–$NaNO_3$ mixtures (Table 1) with $[Cl^-]/[Br^-]$ = 1.0 for (a) χ_{halide} = 0 (4 M $NaNO_3$), (b) χ_{halide} = 0.5, (c) χ_{halide} = 0.75, and (d) χ_{halide} = 0.89.

was located at z = 0 Å. The GDS is defined as the position along the z-axis that is halfway between where the water density is 10% and 90% of the bulk water density. Predicted density profiles for $[Cl^-]/[Br^-]$ = 1.0 (Fig. 4) show that as χ_{halide} increases, nitrate ions are drawn closer to the interface through an electric double layer effect, similar to that predicted[99,100] for the binary NaCl–$NaNO_3$ and NaBr–$NaNO_3$ mixtures. MD simulations for $[Cl^-]/[Br^-]$ = 0.25 and 4.0 showed similar trends in nitrate ion profiles with the halide mole fractions (Fig. S2, ESI†).

The coordination number of water molecules around the nitrate anions is presented in Fig. 5. Fig. 5a shows a direct comparison of the solvation of nitrate ions in the bulk and at the surface for NaCl–$NaNO_3$ (blue triangles) and $[Cl^-]/[Br^-]$ = 4.0 (red squares). As nitrate ions are drawn closer to the interface for

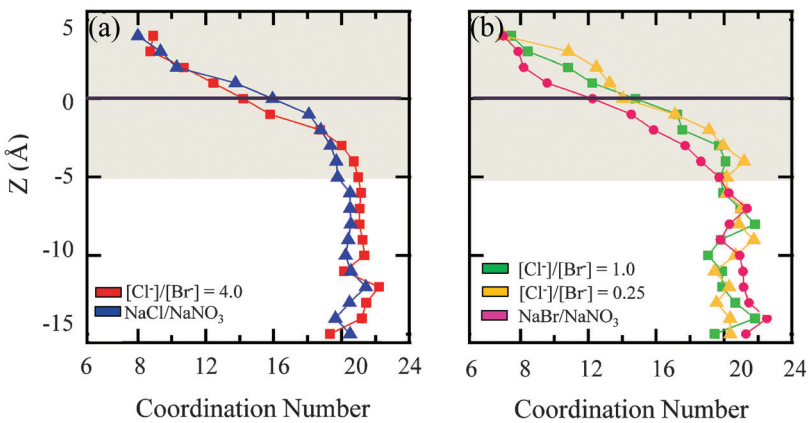

Fig. 5 Number of water molecules within 5.5 Å of the nitrate ion as a function of depth in the slab [Z (Å)] for (a) $[Cl^-]/[Br^-]$ = 4.0 (red) and NaCl–$NaNO_3$ (blue) and (b) $[Cl^-]/[Br^-]$ = 0.25 (orange) and 1.0 (green) and NaBr–$NaNO_3$ (pink). The purple line is the Gibbs dividing surface and the shaded region is the interface region.

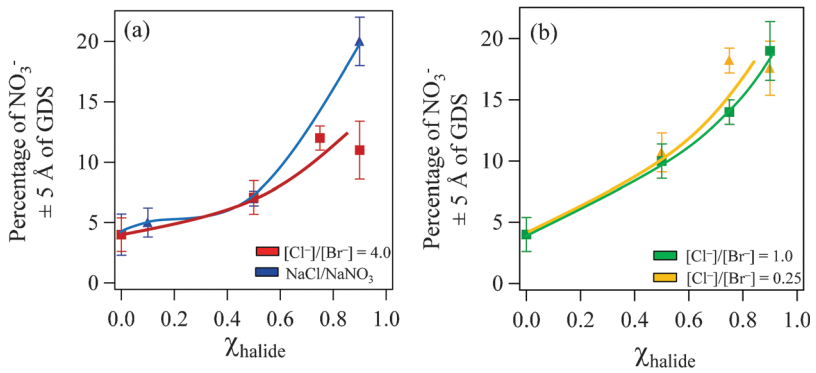

Fig. 6 Predicted percentage of nitrate ions ±5 Å of the Gibbs dividing surface in MD simulations for (a) $[Cl^-]/[Br^-]$ = 4.0 (red) and NaCl–$NaNO_3$ (blue) and (b) $[Cl^-]/[Br^-]$ = 0.25 (orange) and 1.0 (green).

the high chloride experiments, the water solvent cage of nitrate is reduced from twenty-one water molecules (bulk) to seventeen at 3 Å below the GDS and to twelve water molecules at the GDS. Calculations for the high bromide system (Fig. 5b) shows similar behavior to the high chloride system (Fig. 5a), suggesting that the reduction of the solvent cage around nitrate at the interface is playing an important role in the increased production of NO_2 in the presence of halide ions. A detailed discussion of how the solvent cage may affect the quantum yield of nitrate photolysis products is presented in a previous manuscript.[100]

From the data in Fig. 4, the predicted percentages of interfacial nitrate ions, defined as nitrate ions within ±5 Å of the GDS, can be calculated. Fig. 6 shows those percentages as well as those for NaCl–$NaNO_3$[99] as a function of χ_{halide}. Error bars (2*s*) were calculated using the method of block transformations, which provides an estimate of the statistical error in time-correlated data.[120,121] The predicted percentages of NO_3^- in the interfacial region show similar trends to the experimentally measured rates of NO_2 production (Fig. 2a and b). Most significant is the prediction that the percentage of nitrate ions in the interface region is smaller for $[Cl^-]/[Br^-]$ = 4.0 compared to ratios of 1.0 or 0.25, consistent with the experimentally measured enhancement in NO_2 being smaller for this highest ratio of chloride to bromide ions. Thus, the experimentally measured trends in NO_2 production in the presence of halide ions relative to $NaNO_3$ are consistent with the nitrate ion being drawn closer to the interface where it has an incomplete solvent cage, allowing more efficient escape of NO_2 to the gas phase.

The halogen gases Br_2, Cl_2, and BrCl, expected from oxidation of bromide and chloride ions by the reactive intermediates generated in the NO_3^- photolysis, were also monitored as a function of photolysis time using API-MS. The major gas phase halogen observed in all experiments was Br_2, with smaller amounts of BrCl whose yields were consistently 6% of that of Br_2. This is expected given that BrCl undergoes further secondary chemistry in the aqueous phase to form Br_2.[122] No Cl_2 was observed above the detection limit of the instrument (90 ppt). Mass spectra were examined to determine if other halogen-containing species were formed by comparing the ratio of *m*/*z* 81 to *m*/*z* 160 for Br atom species or the ratio of *m*/*z* 35 to *m*/*z* 70 for Cl atom species. There was no evidence of chlorine or bromine species in the mass spectra other than BrCl or Br_2. The lack of formation of Cl_2 is not surprising since inter-halogen chemistry tends to promote the formation of gas phase bromine compounds at the expense of chlorine-containing gases.[60,69,70,123–132] Results by Frinak and Abbatt[60] showed that when NaCl–NaBr mixtures were oxidized by gas phase OH, Cl_2 was not produced until Br^- levels had fallen to $\sim 10^{-5}$ M, where the chloride to bromide ratio was very high, $[Cl^-]/[Br^-] = 3 \times 10^5$.

Fig. 7 shows gas phase Br_2 concentrations as a function of time for $[Cl^-]/[Br^-]$ = 0.25, 1.0 and 4.0, respectively (Fig. 7a–c). Fig. 7d–f shows the corresponding rates of Br_2 formation as well as the ratio of the rates of Br_2 to NO_2 formation. There is an initial induction period for Br_2 formation that is most obvious for the larger ratios of Cl^- to Br^-. The net overall oxidation of Br^- leads to the formation of one Br_2 molecule for every two hydroxyl radicals reacted:

$$2OH + 2Br^- \rightarrow Br_2 + 2OH^- \quad (3)$$

If the photolysis of each NO_3^- generates one NO_2 and one O^-/OH, then the stoichiometric ratio R_{Br_2}/R_{NO_2} should be 0.5. The ratio of the rates of Br_2 to NO_2 formation after the initial induction period (R_{Br_2}/R_{NO_2}) are shown as black open squares in Fig. 7d–f. While there is no trend in R_{Br_2}/R_{NO_2} with χ_{halide}, the stoichiometry falls in the range from $\sim$0.4–0.5, similar to that expected from the overall oxidation reaction (3). This observation is consistent with Br^- or Cl^- efficiently trapping photolytically generated OH, which is limited by the rate of photolysis of NO_3^-. In a somewhat different but related system, irradiated frozen halide–nitrate solutions, Abbatt *et al.*[70] reported the ratio of Br_2 molecules to OH formed was 0.6.

A computational chemical kinetics box model, which includes both gas phase and aqueous bulk phase chemistry of halide and oxides of nitrogen, was used to explore the mechanisms of NO_2 and Br_2 production in the NaCl–NaBr–$NaNO_3$ system. The solid lines in Fig. 8 show the model-predicted NO_2 (Fig. 8a) and Br_2 (Fig. 8b), while the symbols show experimental values. Both the NO_2 and Br_2 data are reasonably well matched by the model. The ratio of the rates of Br_2 production to those for NO_2 predicted by the model for each $[Cl^-]/[Br^-]$ system was very similar to those obtained from the initial experimental rates of NO_2 (Fig. 1) and Br_2 (Fig. 7)

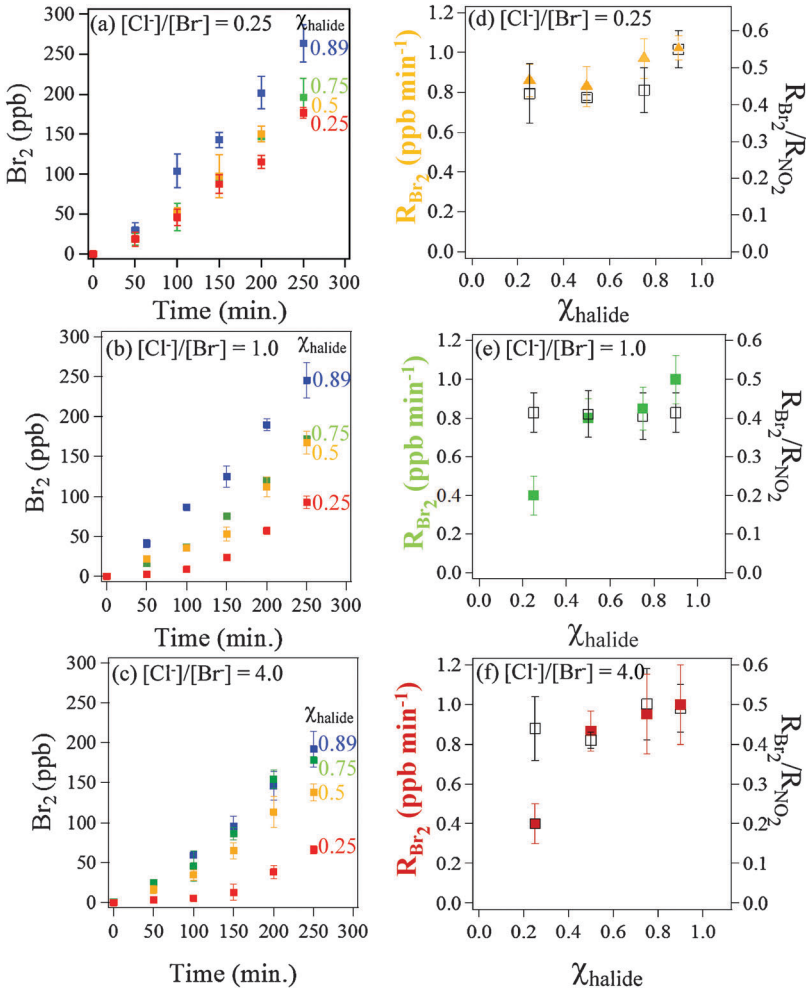

Fig. 7 Parts (a)–(c): gas phase Br_2 concentrations as function of time for $[Cl^-]/[Br^-]$ from 0.25 to 4.0 for different mole fractions χ_{halide}. Parts (d)–(f): rates of Br_2 production (left axis, filled colored symbols) and R_{Br_2}/R_{NO_2} (right axis, black open squares) for $[Cl^-]/[Br^-]$ from 0.25 to 4.0.

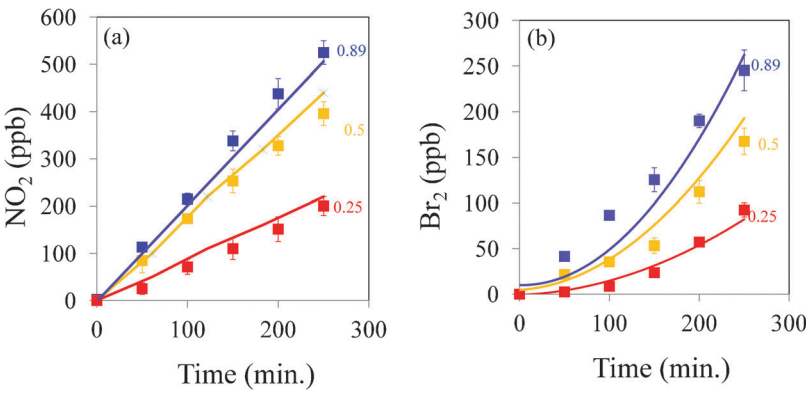

Fig. 8 NO_2 (a) and Br_2 (b) production during photolysis experiments for mixtures of NaCl–NaBr–NaBr for $[Cl^-]/[Br^-] = 1$. Symbols are experimental data and lines represent model-predicted values.

production and is shown in Fig. S3 (ESI†). These results indicate that known bulk phase chemistry is driving Br_2 production, which is dependent on the enhanced rate of NO_2 formation. The total model predicted values for several other gas-phase species ($Cl_2N_2O_5$, ClNO, $ClNO_2$, $ClONO_2$, BrNO, $BrNO_2$ and $BrONO_2$) were <0.25 ppt which is below the detection limits in our system.

The initial induction period for gas phase Br_2 (Fig. 8b) is attributed to bromine compounds being retained in the aqueous phase at high pH which was indicated in the model by a

spike in the OH^- concentration which increased the pH of the film from 5 to 8 during the first fifty minutes of photolysis. The generation of hydroxide ions in reactions (1a) and (2) provides a mechanism for hydrolysis of Br_2 and deprotonation of HOBr in the aqueous phase to BrO^-:

$$Br_2 + OH^- \rightarrow HOBr + Br^- \quad k_4 = 7.0 \times 10^9 \text{ L mol}^{-1} \text{ s}^{-1} \tag{4}$$

$$HOBr \leftrightarrow OBr^- + H^+ \quad pK_a = 8.8^{133} \tag{5}$$

The delay in gas phase Br_2 reflects the time to acidify the film *via* the production of HNO_3 in secondary reactions of the NO_2. In addition to minimizing the hydrolysis of Br_2 in reaction (4), acid converts BrO^- to HOBr and HOBr to Br_2:

$$HOBr + H^+ + Br^- \rightarrow Br_2 + H_2O \quad k_6 = 1.6 \times 10^{10} \text{ L mol}^{-1} \text{ s}^{-1}{}^{134} \tag{6}$$

The delay in Br_2 production was also present in previous NaBr–$NaNO_3$ measurements and our model predicts an increase in OH^- in that system as well.[100]

Das *et al.*[135] suggested that bromide ions could penetrate the nitrate solvent cage and react directly with OH radicals inside the solvent cage, inhibiting the recombination of O^- with NO_2 to regenerate NO_3^-. MD simulations of the NaBr–$NaNO_3$ system predicted significant bromide and nitrate clustering.[100] These clustering events could lead to a direct reaction within the NO_3^-–Br^-–H_2O cluster to form NO_2 + OH^- + $HOBr^-$. Secondary chemistry of $HOBr^-$ can then lead to Br_2 formation (see ESI†). Alternatively, Br^- may react directly with photochemically generated O^-:

$$Br^- + O^- \rightarrow \text{Products} \quad k_7 = 1.8 \times 10^8 \text{ M}^{-1} \text{ s}^{-1}{}^{136} \tag{7}$$

Although the products of reaction (7) have apparently not been reported, O^{2-} + Br seem most likely. Subsequent reactions of bromine atoms generate Br_2 (see Table S3, ESI†). In either case, the back reaction of NO_2 to regenerate NO_3^- would be inhibited, leading to enhanced gas phase NO_2 production.

To further investigate the possible role of such clusters in the chemistry, the percentages of NO_3^- ions coordinated to Cl^- and Br^- were predicted from MD simulations. (It was not possible to obtain adequate sampling for χ_{halide} = 0.25 due to the small number of Cl^- and Br^- ions in the water slab). These clustering events occur both in the bulk and near the interface, and the percentage of nitrate clustering with halide ions increases as χ_{halide} increases (Fig. S4, ESI†). While reaction (7) between O^- and Br^- has been reported,[136] a comparable reaction between O^- and Cl^- has not. Thus, while NO_3^- appears to form clusters according to the simulations with both Cl^- and Br^-, it is unclear whether the chloride clusters will also play a role in the photochemical generation of NO_2 and Br_2. The bromine formed in NaCl–NaBr–$NaNO_3$ was well accounted for by known bulk phase reaction mechanisms as indicated in Fig. 8b suggesting that these clustering events of Br^-–H_2O–NO_3^- are likely a minor source of Br_2 formation.

4. Conclusions

Experimental results show that quantum yields for NO_2 production from nitrate ion photolysis products in thin films containing NaCl–NaBr–$NaNO_3$ are enhanced relative to $NaNO_3$. The increased production of NO_2 is attributed to halide ions drawing Na^+ toward the interface that in turn attracts NO_3^- closer to the interface region where there is a reduced solvent cage. MD simulations of NaCl–NaBr–$NaNO_3$ mixtures show higher concentrations of nitrate ions in the interface region for experiments with excess bromide compared to experiments with excess chloride, consistent with experimental observations of greater enhancements in NO_2 for $[Cl^-]/[Br^-] \leq 1.0$. Our results are consistent with the recent direct observation of enhanced interfacial nitrate ion concentrations due to the presence of bromide ions.[102] It is not clear why glancing-angle Raman experiments do not indicate that chlorides ions also lead to nitrate ion enhancement at the interface. It may be that because these experiments are not exclusively surface sensitive, it may not be possible to detect small enhancements at the surface.

Although the experiments reported here were carried out in an aqueous film at room temperature, the results may provide some insight into the photochemistry on ice surfaces. Nitrate ion photochemistry has been proposed to be a major source of OH and NO_x in snowpacks.[30,38–57,137] Sea salt aerosols are also deposited on the snowpack and can become concentrated in a quasi-liquid layer (QLL) on the surface.[138–140] Based on the present results, halide ions could significantly impact nitrate photochemistry *via* enhanced nitrate ion concentrations at the interface of this QLL. The release of bromine in these experiments by the photolysis of nitrate suggests that enhanced nitrate photochemistry on snowpacks containing sea salt or in aerosols containing halides could be an important source of both NO_x and tropospheric gaseous bromine.

Acknowledgements

This research was supported by the National Science Foundation (Grant #0909227 and #0836735). The authors would like to thank the staff of the Carl Zeiss Center for Excellence in Electron Microscopy at the University of California, Irvine for assistance and access to the facilities. We particularly thank Lisa M. Wingen for her assistance and insightful discussions, Theresa M. McIntire, Christopher W. Dilbeck, Emily Bruns, Veronique Perraud and Mike Ezell for helpful input, Jennie L. Thomas for use of NaCl–$NaNO_3$ raw trajectories and Matthew L. Dawson for providing assistance with the kinetics model. We thank James N. Pitts Jr. for detailed and insightful comments on the manuscript and D. J. Donaldson for sharing data prior to publication.

References

1 R. C. Robbins, R. D. Cadle and D. L. Eckhardt, *J. Meteorol.*, 1959, **16**, 53–56.
2 R. D. Cadle and R. C. Robbins, *Discuss. Faraday Soc.*, 1960, **30**, 155–161.

3 W. H. Schroeder and P. Urone, *Environ. Sci. Technol.*, 1974, **8**, 756–758.
4 B. J. Finlayson-Pitts, *Nature*, 1983, **306**, 676–677.
5 C. Zetzsch, G. Pfahler and W. Behnke, *J. Aerosol Sci.*, 1988, **19**, 1203–1206.
6 B. J. Finlayson-Pitts, M. J. Ezell and J. N. Pitts Jr., *Nature*, 1989, **337**, 241–244.
7 W. Behnke and C. Zetzsch, *J. Aerosol Sci.*, 1989, **20**, 1167–1170.
8 W. Behnke and C. Zetzsch, *J. Aerosol Sci.*, 1990, **21**, S229–S232.
9 W. Behnke, H.-U. Kruger, V. Scheer and C. Zetzsch, *J. Aerosol Sci.*, 1991, **22**, S609–S612.
10 F. E. Livingston and B. J. Finlayson-Pitts, *Geophys. Res. Lett.*, 1991, **18**, 17–21.
11 T. Winkler, J. Goschnick and H. J. Ache, *J. Aerosol Sci.*, 1991, **22**(suppl 1), S605–S608.
12 W. Behnke, V. Scheer and C. Zetzsch, *J. Aerosol Sci.*, 1994, **25**, 277–278.
13 I. M. Msibi, Y. Li, J. P. Shi and R. M. Harrison, *J. Atmos. Chem.*, 1994, **18**, 291.
14 J. M. Laux, J. C. Hemminger and B. J. Finlayson-Pitts, *Geophys. Res. Lett.*, 1994, **21**, 1623–1626.
15 F. F. Fenter, F. Caloz and M. J. Rossi, *J. Phys. Chem.*, 1996, **100**, 1008.
16 H. C. Allen, J. M. Laux, R. Vogt, B. J. Finlayson-Pitts and J. C. Hemminger, *J. Phys. Chem.*, 1996, **100**, 6371–6375.
17 R. Karlsson and E. Ljungström, *J. Aerosol Sci.*, 1995, **26**, 39–50.
18 C. D. Zangmeister and J. E. Pemberton, *J. Phys. Chem. B*, 1998, **102**, 8950.
19 A. Laskin, M. J. Iedema and J. P. Cowin, *Environ. Sci. Technol.*, 2002, **36**, 4948–4955.
20 E. E. Gard, M. J. Kleeman, D. S. Gross, L. S. Hughes, J. O. Allen, B. D. Morrical, D. P. Fergenson, T. Dienes, M. E. Galli, R. J. Johnson, G. R. Cass and K. A. Prather, *Science*, 1998, **279**, 1184–1187.
21 M.-T. Leu, R. S. Timonen, L. F. Keyser and Y. L. Yung, *J. Phys. Chem.*, 1995, **99**, 13203–13212.
22 M. Gershenzon, S. Il'in, N. Fedotov, Y. Gershenzon, E. Aparina and V. Zelenov, *J. Atmos. Chem.*, 1999, **34**, 119–135.
23 C. Zetzsch and W. Behnke, *Ber. Bunsen-Ges. Phys. Chem.*, 1992, **96**, 488–493.
24 *Heterogeneous Reactions of Chlorine Compounds*, ed. C. Zetzsch and W. Behnke, Springer-Verlag, Berlin, 1993.
25 J. R. Arnold and W. T. Luke, *Atmos. Environ.*, 2007, **41**, 4227–4241.
26 M. J. Rossi, *Chem. Rev.*, 2003, **103**, 4823–4882.
27 B. J. Finlayson-Pitts, *Chem. Rev.*, 2003, **103**, 4801–4822.
28 B. J. Finlayson-Pitts, *Anal. Chem.*, 2009, **82**, 770–776.
29 B. J. Finlayson-Pitts and J. N. Pitts Jr, *Chemistry of the Upper and Lower Atmosphere – Theory, Experiments, and Applications*, Academic Press, San Diego, 2000.
30 C. Anastasio and J. T. Newberg, *J. Geophys. Res.*, 2007, **112**, D10306, DOI: 10310.11029/12006JD008061.
31 J. E. Dibb and J.-L. Jaffrezo, *J. Geophys. Res., Oceans*, 1997, **102**, 26795–26807.
32 S. Whitlow, P. A. Mayewski and J. E. Dibb, *Atmos. Environ.*, 1992, **26**, 2045–2054.
33 J. Mack and J. R. Bolton, *J. Photochem. Photobiol., A*, 1999, **128**, 1–13.
34 R. G. Zepp, J. Hoigne and H. Bader, *Environ. Sci. Technol.*, 1987, **21**, 443–450.
35 R. Zellner, M. Exner and H. Herrmann, *J. Atmos. Chem.*, 1990, **10**, 411–425.
36 P. Warneck and C. Wurzinger, *J. Phys. Chem.*, 1988, **92**, 6278–6283.
37 H. Herrmann, *Phys. Chem. Chem. Phys.*, 2007, **9**, 3935–3964.
38 J. Bock and H.-W. Jacobi, *J. Phys. Chem. A*, 2010, **114**, 1790–1796.
39 D. Davis, J. B. Nowak, G. Chen, M. Buhr, R. Arimoto, A. Hogan, F. Eisele, L. Mauldin, D. Tanner, R. Shetter, B. Lefer and P. McMurry, *Geophys. Res. Lett.*, 2001, **28**, 3625–3628.
40 A. L. Sumner and P. B. Shepson, *Nature*, 1999, **398**, 230–233.
41 E. W. Wolff, A. E. Jones, T. J. Martin and T. C. Grenfell, *Geophys. Res. Lett.*, 2002, **29**, 1944–1948.
42 E. S. Galbavy, C. Anastasio, B. Lefer and S. Hall, *Atmos. Environ.*, 2007, **41**, 5091–5100.
43 R. E. Honrath, M. C. Peterson, S. Guo, J. E. Dibb, P. B. Shepson and B. Campbell, *Geophys. Res. Lett.*, 1999, **26**, 695–698.
44 A. E. Jones, R. Weller, P. S. Anderson, H.-W. Jacobi, E. W. Wolff, O. Schrems and H. Miller, *Geophys. Res. Lett.*, 2001, **28**, 1499–1502.
45 A. M. Grannas, A. E. Jones, J. Dibb, M. Ammann, C. Anastasio, H. J. Beine, M. Bergin, J. Bottenheim, C. S. Boxe, G. Carver, G. Chen, J. H. Crawford, F. Domine, M. M. Frey, M. I. Guzman, D. E. Heard, D. Helmig, M. R. Hoffmann, R. E. Honrath, L. G. Huey, M. Hutterli, H. W. Jacobi, P. Klan, B. Lefer, J. McConnell, J. Plane, R. Sander, J. Savarino, P. B. Shepson, W. R. Simpson, J. R. Sodeau, R. von Glasow, R. Weller, E. W. Wolff and T. Zhu, *Atmos. Chem. Phys.*, 2007, **7**, 4329–4373.
46 X. Zhou, H. J. Beine, R. E. Honrath, J. D. Fuentes, W. Simpson, P. B. Shepson and J. W. Bottenheim, *Geophys. Res. Lett.*, 2001, **28**, 4087–4090.
47 R. E. Honrath, M. C. Peterson, M. P. Dziobak, J. E. Dibb, M. A. Arsenault and S. A. Green, *Geophys. Res. Lett.*, 2000, **27**, 2237–2240.
48 A. E. Jones, R. Weller, E. W. Wolff and H.-W. Jacobi, *Geophys. Res. Lett.*, 2000, **27**, 345–348.
49 D. Davis, G. Chen, M. Buhr, J. Crawford, D. Lenschow, B. Lefer, R. Shetter, F. Eisele, L. Mauldin and A. Hogan, *Atmos. Environ.*, 2004, **38**, 5375–5388.
50 R. E. Honrath, S. Guo, M. C. Peterson, M. P. Dziobak, J. E. Dibb and M. A. Arsenault, *J. Geophys. Res.*, 2000, **105**, 24183–24190.

51 C. S. Boxe, A. J. Colussi, R. C. Hoffman, I. M. Perez, J. G. Murphy and R. C. Cohen, *J. Phys. Chem. A*, 2006, **110**, 3578–3583.
52 Y. Dubowski, A. J. Colussi, C. Boxe and M. R. Hoffmann, *J. Phys. Chem. A*, 2002, **106**, 6967–6971.
53 L. Chu and C. Anastasio, *J. Phys. Chem. A*, 2003, **107**, 9594–9602.
54 A. Yabushita, D. Iida, T. Hama and M. Kawasaki, *J. Phys. Chem. A*, 2008, **112**, 9763–9766.
55 A. Yabushita, N. Kawanaka, M. Kawasaki, P. D. Hamer and D. E. Shallcross, *J. Phys. Chem. A*, 2007, **111**, 8629–8634.
56 H.-W. Jacobi, T. Annor and E. Quanash, *J. Photochem. Photobiol., A*, 2006, **179**, 330–338.
57 O. Abida and H. D. Osthoff, *Geophys. Res. Lett*, 2011, **38**, L16808.
58 G. V. Buxton, *Trans. Faraday Soc.*, 1970, **66**, 1656–1660.
59 W. Behnke, M. Elend, U. Kruger and C. Zetzsch, *J. Atmos. Chem.*, 1999, **34**, 87–99.
60 E. K. Frinak and J. P. D. Abbatt, *J. Phys. Chem. A*, 2006, **110**, 10456–10464.
61 C. Anastasio and M. Mozurkewich, *J. Atmos. Chem.*, 2002, **41**, 135–162.
62 D. O. DeHaan, T. Brauers, K. Oum, J. Stutz, T. Nordmeyer and B. J. Finlayson-Pitts, *Int. Rev. Phys. Chem.*, 1999, **18**, 343–385.
63 M. S. Matheson, W. A. Mulac, J. L. Weeks and J. Rabani, *J. Phys. Chem.*, 1966, **70**, 2092–2099.
64 G. G. Jayson, B. J. Parsons and A. J. Swallow, *J. Chem. Soc., Faraday Trans.*, 1973, **69**, 1597–1607.
65 D. Zehavi and J. Rabani, *J. Phys. Chem.*, 1972, **76**, 312.
66 H. C. Sutton, G. E. Adams, J. W. Boag and B. D. Michael, *Pulse Radiolysis Academic Press*, London, 1965, pp. 61–81.
67 U. von Gunten and J. Hoigne, *Environ. Sci. Technol.*, 1994, **28**, 1234–1242.
68 U. von Gunten and Y. Oliveras, *Environ. Sci. Technol.*, 1998, **32**, 63–70.
69 I. J. George and C. Anastasio, *Atmos. Environ.*, 2007, **41**, 543–553.
70 J. Abbatt, N. Oldridge, A. Symington, V. Chukalovskiy, R. D. McWhinney, S. Sjostedt and R. A. Cox, *J. Phys. Chem. A*, 2010, **114**, 6527–6533.
71 P. Nissenson, L. M. Wingen, S. W. Hunt, B. J. Finlayson-Pitts and D. Dabdub, *Atmos. Environ.*, 2013, submitted for publication.
72 W. C. Keene, A. A. P. Pszenny, D. J. Jacob, R. A. Duce, J. N. Galloway, J. J. Schultz-Tokos, H. Sievering and J. F. Boatman, *Global Biogeochem. Cycles*, 1990, **4**, 407–430.
73 R. Sander, W. C. Keene, A. A. P. Pszenny, R. Arimoto, G. P. Ayers, E. Baboukas, J. M. Cainey, P. J. Crutzen, R. A. Duce, G. Hönninger, B. J. Huebert, W. Maenhaut, N. Mihalopoulos, V. C. Turekian and R. V. Dingenen, *Atmos. Chem. Phys.*, 2003, **3**, 1301–1336.
74 R. von Glasow and P. J. Crutzen, in *Treatise on Geochemistry, Update 1*, ed. H. D. Holland and K. Turekian, 2007, pp. 1–67.
75 L. A. Barrie, J. W. Bottenheim, R. C. Schnell, P. J. Crutzen and R. A. Rasmussen, *Nature*, 1988, **334**, 138–141.
76 K. L. Foster, R. A. Plastridge, J. W. Bottenheim, P. B. Shepson, B. J. Finlayson-Pitts and C. W. Spicer, *Science*, 2001, **291**, 471–474, DOI: 10.1126/science.1291.5503.1471.
77 W. R. Simpson, U. von Gunten, K. Riedel, P. Anderson, P. Ariya, J. Bottenheim, J. Burrows, L. J. Carpenter, U. FrieB, M. E. Goodsite, D. Heard, M. Hutterli, H.-W. Jacobi, L. Kaleschke, B. Neff, J. Plane, U. Platt, A. Ritcher, H. Roscoe, R. Sander, P. B. Shepson, J. Sodeau, A. Steffen, T. Wagner and E. W. Wolff, *Atmos. Chem. Phys.*, 2007, **7**, 4375–4418.
78 E. Tas, M. Peleg, D. U. Pedersen, V. Matveev, A. Pour Biazar and M. Luria, *Atmos. Chem. Phys.*, 2006, **6**, 5589–5604.
79 R. R. Dickerson, K. P. Rhoads, T. P. Carsey, S. J. Oltmans, J. P. Burrows and P. J. Crutzen, *J. Geophys. Res.*, 1999, **104**, 21385–21395.
80 I. Nagao, K. Matsumoto and H. Tanaka, *Geophys. Res. Lett.*, 1999, **26**, 3377–3380.
81 I. E. Galbally, S. T. Bentley and C. P. Meyer, *Geophys. Res. Lett.*, 2000, **27**, 3841–3844.
82 C. W. Spicer, R. A. Plastridge, K. L. Foster, B. J. Finlayson-Pitts, J. W. Bottenheim, A. M. Grannas and P. B. Shepson, *Atmos. Environ.*, 2002, **36**, 2721–2731.
83 G. A. Impey, P. B. Shepson, D. R. Hastie, L. A. Barrie and K. G. Anlauf, *J. Geophys. Res.*, 1997, **102**, 16005–16010.
84 W. R. Simpson, R. von Glasow, K. Riedel, P. Anderson, P. Ariya, J. Bottenheim, J. Burrows, L. Carpenter, U. Frieb, M. E. Goodsite, D. Heard, M. Hutterli, H.-W. Jacoi, L. Kaleschke, B. Neff, J. Plane, U. Platt, A. Richter, H. Roscoe, R. Sander, P. Shepson, J. Sodeau, A. Steffen, T. Wagner and E. Wolff, *Atmos. Chem. Phys.*, 2007, **7**, 4375–4418.
85 J. W. Bottenheim, A. G. Gallant and K. A. Brice, *Geophys. Res. Lett.*, 1986, **13**, 113–116.
86 K. Hebestreit, J. Stutz, D. Rosen, M. Peleg, V. Matveiv, M. Luria and U. Platt, *Science*, 1999, **283**, 55–57.
87 J. Stutz, R. Ackermann, J. D. Fast and L. Barrie, *Geophys. Res. Lett.*, 2002, **29**, 1380–1383.
88 E. M. Knipping and D. Dabdub, *J. Geophys. Res.*, 2002, **107**, 4360.
89 S. Pechtl and R. von Glasow, *Geophys. Res. Lett.*, 2007, **34**, 11813.
90 W. L. Chameides and A. W. Stelson, *J. Geophys. Res.*, 1992, **97**, 20565–20580.
91 C. W. Spicer, E. G. Chapman, B. J. Finlayson-Pitts, R. A. Plastridge, J. M. Hubbe, J. D. Fast and C. W. Berkowitz, *Nature*, 1998, **394**, 353–356.
92 D. J. Erickson, C. Seuzaret, W. C. Keene and S. L. Gong, *J. Geophys. Res.*, 1999, **104**, 8347–8372.
93 R. Sander and P. J. Crutzen, *J. Geophys. Res.*, 1996, **101**, 9121–9138.
94 R. Sander, R. Vogt, G. W. Harris and P. J. Crutzen, *Tellus Ser. B*, 1997, **49**, 522–532.
95 R. von Glasow, R. Sander, A. Bott and P. J. Crutzen, *J. Geophys. Res.*, 2002, **107**, 4341.
96 H. D. Osthoff, J. M. Roberts, A. R. Ravishankara, E. J. Williams, B. M. Lerner, R. Sommariva, T. S. Bates,

D. Coffman, P. K. Quinn, J. E. Dibb, H. Stark, J. B. Burkholder, R. K. Talukdar, J. Maegher, F. C. Fehsenfeld and S. S. Brown, *Nat. Geosci.*, 2008, **1**, 323–328.
97 H. Simon, Y. Kimura, G. McGaughey, D. T. Allen, S. S. Brown, D. Coffman, J. E. Dibb, H. D. Osthoff, P. K. Quinn, J. M. Roberts, G. Yarwood, S. Kemball-Cook, D. Byun and D. Lee, *Atmos. Environ.*, 2009, **44**, 5476–5488.
98 M. J. Lawler, R. Sander, L. J. Carpenter, J. D. Lee, R. von Glasow, R. Sommariva and E. S. Saltzman, *Atmos. Chem. Phys.*, 2011, **11**, 7617–7628.
99 L. M. Wingen, A. C. Moskun, S. N. Johnson, J. L. Thomas, M. Roeselova, J. Tobias, D. M. T. Kleinman and B. J. Finlayson-Pitts, *Phys. Chem. Chem. Phys.*, 2008, 5668.
100 N. K. Richards, L. M. Wingen, K. M. Callahan, N. Nishino, M. T. Kleinman, D. J. Tobias and B. J. Finlayson-Pitts, *J. Phys. Chem. A*, 2011, **115**, 5810–5821.
101 N. K. Richards and B. J. Finlayson-Pitts, *Environ. Sci. Technol.*, 2012, **46**, 10447–10454.
102 C. Hong, S. N. Wren and D. J. Donaldson, *J. Phys. Chem. Lett.*, 2013, **4**, 2994–2998.
103 J. U. White, *J. Opt. Soc. Am.*, 1942, **32**, 285–288.
104 D. A. Skoog, F. J. Holler and T. A. Nieman, *Principles of Instrumental Analysis*, Saunders College Publishing, Philadelphia, 5th edn, 1998.
105 M. A. Wilson, A. Pohorille and L. R. Pratt, *J. Phys. Chem.*, 1987, **91**, 4873.
106 I. Benjamin, *J. Chem. Phys.*, 1991, **95**, 3698.
107 M. P. Allen and D. J. Tildesley, *Computer Simulation of Liquids*, Clarendon, Oxford, 1987.
108 H. J. C. Berendsen, J. P. M. Postma, W. F. Vangunsteren, A. Dinola and J. R. Haak, *J. Chem. Phys.*, 1984, **81**, 3684.
109 J. W. Caldwell and P. A. Kollman, *J. Phys. Chem.*, 1995, **99**, 6208.
110 J. P. Ryckaert, G. Ciccotti and H. J. C. Berendsen, *J. Comput. Phys.*, 1977, **23**, 327.
111 L. S. Sremaniak, L. Perera and M. L. Berkowitz, *Chem. Phys. Lett.*, 1994, **218**, 377–382.
112 L. Perera and M. L. Berkowitz, *J. Chem. Phys.*, 1994, **100**, 3085.
113 J. L. Thomas, M. Roeselová, L. X. Dang and D. J. Tobias, *J. Phys. Chem. A*, 2007, **111**, 3091.
114 B. Minofar, R. Vacha, A. Wahab, S. Mahiuddin, W. Kunz and P. Jungwirth, *J. Phys. Chem. B*, 2006, **110**, 15939.
115 P. Salvador, J. E. Curtis, D. J. Tobias and P. Jungwirth, *Phys. Chem. Chem. Phys.*, 2003, **5**, 3752.
116 D. A. Case, T. A. Darden, T. E. Cheatham III, C. L. Simmerling, J. Wang, R. E. Duke, R. Luo, K. M. Merz, B. Wang, D. A. Pearlman, M. Crowley, S. Brozell, V. Tsui, H. Gohlke, J. Mongan, V. Hornak, G. Cui, P. Beroza, C. Schafmeister, J. W. Caldwell, W. S. Ross and P. A. Kollman, University of California, San Francisco, 2004.
117 P. B. Petersen, R. J. Saykally, M. Mucha and P. Jungwirth, *J. Phys. Chem. B*, 2005, **109**, 10915.
118 T. Darden, D. York and L. Pedersen, *J. Chem. Phys.*, 1993, **98**, 10089.
119 U. Essmann, L. Perera, M. L. Berkowitz, T. Darden, H. Lee and L. G. Pedersen, *J. Chem. Phys.*, 1995, **103**, 8577.
120 H. Flybjerg and H. G. Petersen, *J. Chem. Phys.*, 1989, **91**, 461–466.
121 R. W. Benz, F. Castro-Romain, D. J. Tobias and S. H. White, *Biophys. J.*, 2005, **88**, 805–817.
122 T. X. Wang and D. W. Margerum, *Inorg. Chem.*, 1994, **33**, 1050–1055.
123 Q. Liu, L. M. Schurter, C. E. Muller, S. Aloisio, J. S. Francisco and D. W. Margerum, *Inorg. Chem.*, 2001, **40**, 4436.
124 S. J. Sjostedt and J. P. D. Abbatt, *Environ. Res. Lett.*, 2008, **3**, 045007.
125 J. P. D. Abbatt, *Geophys. Res. Lett.*, 1994, **21**, 665–668.
126 J. P. D. Abbatt and G. C. G. Waschewsky, *J. Phys. Chem. A*, 1998, **102**, 3719–3725.
127 A. Allanic, R. Oppliger and M. J. Rossi, *J. Geophys. Res.*, 1997, **102**, 23529–23541.
128 L. Chu and L. T. Chu, *J. Phys. Chem. A*, 1999, **103**, 8640–8649.
129 S. Fickert, J. W. Adams and J. N. Crowley, *J. Geophys. Res.*, 1999, **104**, 23719–23727.
130 U. Kirchner, T. H. Benter and R. N. Schindler, *Ber. Bunsen–Ges. Phys. Chem.*, 1997, **101**, 975–977.
131 M. Mochida, H. Akimoto, H. van den Bergh and M. J. Rossi, *J. Phys. Chem. A*, 1998, **102**, 4819–4828.
132 K. W. Oum, M. J. Lakin and B. J. Finlayson-Pitts, *Geophys. Res. Lett.*, 1998, **25**, 3923–3926.
133 W. R. Haag and J. Hoigne, *Environ. Sci. Technol.*, 1983, **17**, 261–267.
134 R. C. Beckwith, T. X. Wang and D. W. Margerum, *Inorg. Chem.*, 1996, 995.
135 R. Das, B. K. Dutta, V. Maurino, D. Vione and C. Minero, *Environ. Chem. Lett.*, 2009, **7**, 337–342.
136 D. Zehavi and J. Rabani, *J. Phys. Chem.*, 1971, **75**, 1738–1744.
137 C. S. Boxe and A. Saiz-Lopez, *Atmos. Chem. Phys.*, 2008, **8**, 4855–4864.
138 T. Koop, A. Kapilashrami, L. T. Molina and M. J. Molina, *J. Geophys. Res.*, 2000, **105**, 26393–26402.
139 H. Cho, P. B. Shepson, L. A. Barrie, J. P. Cowin and R. Zaveri, *J. Phys. Chem. B*, 2002, **106**, 11226–11232.
140 A. Bogdan, M. Kulmala, A. R. MacKenzie and A. Laaksonen, *J. Geophys. Res.*, 2003, **108**, 4303.

